Desalination and Water Treatment
www.deswater.com
doi: 10.1080/19443994.2014.960456

56 (2015) 2402–2416
November

Taylor & Francis
Taylor & Francis Group

Low-temperature stabilization of electrosynthesized tetragonal zirconia, its photoactivity toward methylene blue decolorization

A.A. Jalil[a,b,*], S. Triwahyono[c,d], N. Sapawe[b], I.H. Ahmed[b], M.A.A. Aziz[b]

[a]*Institute of Hydrogen Economy, Universiti Teknologi Malaysia, 81310 UTM Johor Bahru, Johor, Malaysia, Tel. +60 7 5535581; Fax: +60 7 5588166; email: aishah@cheme.utm.my (A.A. Jalil)*
[b]*Faculty of Chemical Engineering, Department of Chemical Engineering, Universiti Teknologi Malaysia, 81310 UTM Johor Bahru, Johor, Malaysia*
[c]*Institute of Ibnu Sina for Fundamental Science Studies, Universiti Teknologi Malaysia, 81310 UTM Johor Bahru, Johor, Malaysia*
[d]*Faculty of Science, Department of Chemistry, Universiti Teknologi Malaysia, 81310 UTM Johor Bahru, Johor, Malaysia*

Received 6 December 2013; Accepted 25 August 2014

ABSTRACT

Zirconia nanoparticles (ZrO_2) were prepared by a simple electrochemical method and characterized using X-ray diffraction, transmission electron microscopy, Brunnauer–Emmett–Teller surface area analysis, and ultraviolet-visible diffuse reflectance spectroscopy. In this study, tetragonal ZrO_2 (*t*-ZrO_2) particles were stabilized at a lower calcination temperature without the addition of a dopant in the preparation step. It was suggested that the use of tetraethylammonium perchlorate as the supporting electrolyte was responsible for the stabilization of *t*-ZrO_2 by preventing the agglomeration of metal clusters with undesired powders in the electrolysis system, resulting in a decrease in ZrO_2 crystal size. The photoactivity of the catalyst was optimized using central composite design with response surface methodology and the optimum values of the parameters were a solution pH of 11, contact time of 4 h, catalyst dosage of 1.0 g L^{-1}, and calcination temperature of 523 K. This resulted in 84.9% decolorization of methylene blue (MB) obtained from the predicted model, which fitted well with the laboratory results of 83.6%. The kinetics study demonstrates that the reaction followed pseudo first-order kinetics, and the rate constants K_R = 0.09 mg L^{-1} h^{-1} and K_{LH} = 0.43 L mg^{-1} were determined using the Langmuir–Hinshelwood model. The mineralization of MB was measured by chemical oxygen demand removal, BOD_5/COD, and TOC/TOC_0 ratio analyses with values of 78.5%, 1.48, and 0.21, respectively, after 4 h of contact time. The regeneration study shows that the catalyst could be maintained with a slight decrease in decolorization (<10%) after five cycling runs. Furthermore, *t*-ZrO_2 facilitated good photoactivity towards MB decolorization under UV light in a batch reactor compared with commercial *t*-ZrO_2 (58.7%) and Degussa P25 TiO_2 (64.5%).

Keywords: t-ZrO_2; Electrochemical; Central composite design; Photodecolorization; Methylene blue

*Corresponding author.

1. Introduction

Industrial dyestuffs constitute one of the largest groups of organic compounds that represent an increasing environmental hazard [1]. Since dyes have the characteristic that they provide bright and lasting color to other substances, the discharge of these highly colored wastes is not only aesthetically unpleasant but also hinders light penetration, hence upsetting biological processes in the receiving water body [2,3]. As a consequence, different strategies have been devised for the removal of these pollutants from water. Conventional biological and physical treatment methods are ineffective because they are time consuming and lead to the generation of secondary pollutants [4–11].

Advanced oxidation processes (AOPs) have been proposed as an attractive alternative for the treatment of contaminated ground, surface, and wastewater containing organic pollutants [12]. Among these AOPs, the use of semiconductor metal oxides, such as TiO_2, ZnO, Fe_2O_3, ZrO_2, and CuO, have become popular in recent years because they can convert various types of dye compounds into nontoxic products, for example CO_2 and water, at ambient temperatures [2,3,13–20]. These methods are generally based on the generation of OH radicals which interact with organic pollutants, leading to progressive degradation and subsequently complete mineralization [21–24].

Zirconia (ZrO_2) nanoparticles have attracted much interest due to their specific optical and electrical properties and potential applications in transparent and optical devices, sensors, fuel cell, advanced ceramics as well as photocatalysts [2,25]. Since the pure tetragonal phase is more catalytically active than a combination of the tetragonal and monoclinic phases [26,27], special attention has been paid to its preparation, particularly at low temperatures [28]. Table 1 shows several methods for the preparation of *t*-ZrO_2, including the precipitation, sol–gel, hydrothermal, and pyrolysis processes conducted under different calcination temperatures [25,29–36]. These data demonstrate that several investigators have succeeded in preparing *t*-ZrO_2 at low temperature, with the lowest temperature of 673 K. However, a simple procedure without the need for complicated apparatus or experimental setup, the absence of any dopants, low impurity, and fewer production steps is still required in order to attain a high-throughput and cost-effective method. The production of *t*-ZrO_2 nanoparticles with high surface area and crystallinity is also crucial in enhancing photocatalytic activity.

Recently, we reported a new preparation method for α-Fe_2O_3, ZrO_2, and CuO supported HY catalysts by a simple and rapid electrochemical process, which possess high photoactivity in the decolorization of methyl orange, methylene blue, and malachite green, respectively [2,3,37]. In addition, we found that the ZnO prepared by the same method led to the generation of nanoparticles, which are less than 30 nm in size that distributed on the surface of HY support, resulting in the enhancement of methylene blue decolorization [38]. These findings led to an interest in exploring the synthesis of a nanosized tetragonal phase of ZrO_2 by the corresponding method, focusing on the effect of calcination temperature. To the best of our knowledge, there is no similar report on the preparation of a pure *t*-ZrO_2 phase. Therefore, in this study, we report for the first time the electrosynthesis of a stabilized *t*-ZrO_2 phase underwent subsequent calcination at low temperature (Table 1). The prepared ZrO_2 particles were then characterized by X-ray diffraction (XRD), transmission electron microscopy (TEM), energy dispersive X-ray (EDX), Brunnauer–Emmett–Teller surface area analysis (BET), and ultraviolet-visible diffuse reflectance spectroscopy (UV–vis/DRS). The performance of the *t*-ZrO_2 catalyst was examined and optimized for the photodecolorization of methylene blue (MB) using

Table 1
Comparison of the method preparation of *t*-ZrO_2 under different calcination temperature

No.	Method preparation	Temperature calcination (K)	References
1	Single emulsion-assisted direct precipitation	1,073	[23]
2	sol–gel–hydrothermal	673	[27]
3	Sol-gel	673	[28]
4	Hydroxide–gel	673	[29]
5	Surfactant-assisted route	873	[30]
6	Non-alkoxide sol–gel	973	[31]
7	Microwave assisted sol–gel	723	[32]
8	Silica bath/co-precipitation	1,173	[33]
9	Spray pyrolysis	873	[34]
10	Electrochemical	523	This study

central composite design (CCD) with response surface methodology (RSM). The interaction effects of four operational variables (factors), including pH (x_1), contact time (x_2), catalyst dosage (x_3), and calcination temperature (x_4), were investigated, with the percentage decolorization of methylene blue (MB) chosen as the output variable (response). Model validation for experimental confirmation was also conducted to study the effects regarding the decolorization of MB. The kinetics, regeneration, and biodegradability of the system were also discussed in detail.

2. Experimental

2.1. Materials

N,*N*-dimethylformamide (DMF) was purchased from Merck Sdn. Bhd., Malaysia and naphthalene was obtained from Fluka, Malaysia. Sodium hydroxide (NaOH), hydrochloric acid (HCl), and methylene blue (C.I. 52015 for microscopy) were obtained from QReC™. The platinum (Pt) and zirconia (Zr) plate cells were obtained from Nilaco Metal, Japan; *t*-ZrO_2 was acquired from Wako Pure Chemical, whereas Degussa P25 TiO_2 was obtained from Acros Organics, Belgium. All reagents were of analytical grade and were used as received. Deionized water was used for the preparation of the pH solution and pH adjustments were performed using 0.1 M HCl and NaOH solutions.

2.2. Catalyst preparation

The ZrO_2 catalyst was prepared via a procedure reported in the literature [39–41]. A 10 mL DMF solution containing 0.1 M tetraethylammonium perchlorate (TEAP) was electrolyzed in the presence of 6 mmol naphthalene as a mediator in a one-compartment cell fitted with a Pt plate cathode ($2 \times 2\ cm^2$) and a Zr plate anode ($2 \times 2\ cm^2$), at a constant current density of $120\ mA/cm^2$ under a nitrogen atmosphere at 273 K. Naphthalene was used as a mediator in the system to produce radical anions, which then reduced the zirconia cations from the anode to give zirconia nanoparticles (Zr^0). After electrolysis, the mixture was impregnated and oven dried overnight at 378 K, and calcined at 523, 823, and 1,123 K for 3 h to give a white powder, ZrO_2, which was ready for characterization and photocatalytic testing.

2.3. Characterization

The crystalline structures of the catalysts were studied by XRD recorded on a D8 ADVANCE Bruker X-ray diffractometer using Cu K_α radiation at a 2θ angle ranging from 3° to 90°. The particle sizes of the catalysts were calculated using the Debye–Scherrer equation:

$$D = \frac{k\lambda}{\beta \cos \theta} \quad (1)$$

where k = 0.94 is the coefficient, λ = 1.5406 Å is the X-ray wavelength, β is the full width half maximum of the sample and θ is the diffracting angle. The phases were identified with the aid of files provided by the Joint Committee on Powder Diffraction Standards (JCPDS).

The morphological properties of the ZrO_2 catalyst were examined by TEM (JEOL JEM-2100F). The textural properties were determined from nitrogen adsorption–desorption isotherms at the temperature of liquid nitrogen using a Micromeritics ASAP 2010 instrument. The nitrogen adsorption–desorption isotherm and Barrett–Joyner–Halender (BJH) pore distributions were calculated from the desorption branch of the nitrogen isotherm of the samples. Prior to measurement, all the samples were degassed at 383 K to 0.1 Pa. The optical absorption properties of the catalyst were obtained using a UV–vis DRS (Perkin Elmer Spectrophotometer) in the range of 200–800 nm at room temperature. The band gap of ZrO_2 was determined from plots of the Kubelka–Munk (K–M) function [$f_{K-M} = (h\upsilon/\lambda)^{1/2}$] as a function of the energy of the excitation light [$h\nu$].

2.4. Photocatalytic testing

The photocatalytic activity of the prepared ZrO_2 catalyst was tested by the decolorization of MB. A 0.2 g sample of the ZrO_2 was dispersed in 200 mL of 10 mg L^{-1} MB aqueous solution. The adsorption–desorption equilibrium was achieved under dark conditions after 2 h, and the mixture was irradiated at room temperature for 5 h with constant stirring using a UV lamp (VL-208 BL; 2 × 8 W, 365 nm tube; power 32 W (Vilber Lourmat, France)). During the irradiation, the suspensions were sampled out (2.5 mL) at specific time intervals. Before analysis, the aqueous suspension was centrifuged to remove any suspended solid catalyst particles. Then, absorption spectrum of the clear solution was recorded using a UV–vis spectrophotometer (Genesys 10 UV Scanning, Thermo Scientific) and the decolorization extent was calculated in terms of the change in the absorbance at the λ_{max} = 664 nm. The decolorization percentage was calculated as follows:

$$\text{Decolorization } (\%) = \frac{(C_0 - C_t)}{C_0} \times 100 \quad (2)$$

where C_0 represents the initial concentration and C_t denotes the variable concentration.

2.5. Experimental design and optimization

The effects of the operating parameters were optimized using RSM. RSM is a set of mathematical and statistical methods for designing experiments, constructing models, evaluating the effects of variables, and seeking optimum conditions of variables to predict targeted responses. The application of statistical experimental design techniques in photocatalytic processes could result in improved photodecolorization activity, reduced process variability, closer confirmation of the output response to nominal and targeted requirements, and reduced development time and overall costs [42–44].

In this study, CCD was selected for RSM in the experimental design, which was a good match for the fitting of a quadratic surface and worked well for the optimization of the process. The CCD is an effective design that is ideal for sequential experimentation and allows a reasonable amount of information for testing lack of fit while not involving an unusually large number of design points [42].

A set of 26 runs (including two replications) were designed to optimize the photodecolorization of MB using ZrO_2. The four independent variables studied were the pH (x_1), contact time (x_2), catalyst dosage (x_3), and calcination temperature (x_4), whereas the decolorization of MB was chosen as the output variable (response). The ranges and levels of the independent variables studied were determined through a series of preliminary evaluations and are presented in Table 2. Statistica software (version 6.0.591.0, StatSoft, Inc., Tulsa, OK, USA) was used for regression and graphical analyses of the data. In the optimization process, the experimental responses can be analyzed with the following second order polynomial:

$$Y = \beta_o + \sum_{i=1}^{k} \beta_j X_j + \sum_{i=1}^{k} \beta_{jj} X_j^2 + \sum_{i<j}^{k} \beta_{ij} X_i X_j \quad (3)$$

where Y = response (percentage decolorization, %), X_i and X_j = variables, β_0 = constant

coefficient β_j, β_{jj}, and β_{ij} = interaction coefficients of linear, quadratic, and second order terms, respectively, and k is the number of studied factors. The quality of the polynomial model fit was expressed by the value of the correlation coefficient (R^2). The equation was validated by analysis of variance (ANOVA) to determine the significance of each term in the fitted equation and to estimate the correlation of each term [42].

Table 2
Independent variables and their respective coded levels used in the CCD design

Variables	Factors	Actual values for coded levels		
		–1	0	+1
pH	x_1	3	7	11
Contact time (h)	x_2	1	3	5
Catalyst dosage (g L^{-1})	x_3	0.1	0.4	1.0
Calcination temperature (K)	x_4	523	823	1,123

3. Results and discussion

3.1. Characterization

3.1.1. Crystallinity, phase, and structural studies

The XRD pattern of the prepared ZrO_2 catalyst was compared for each calcination temperature, and shown in Fig. 1(a). The zirconium oxide seemed amorphous in nature at 378 K. When ZrO_2 was calcined at 523 K, a series of characteristic peaks were observed at 31.5˚ (101), 35˚ (110), 50˚ (112), and 60˚ (211) which are consistent with the tetragonal phase of ZrO_2 (JCPDS File PDF No. 01-072-2743). However, at 823 K, in addition to the peaks corresponding to t-ZrO_2, other characteristic peaks were also observed at 2θ equal to 18˚, 24˚, 28˚, 31.5˚, 34.5˚, 35.5˚, 41˚, 45˚, 49˚, 55˚, 56.5˚, 63˚, and 65.5˚, which corresponded to the diffraction patterns of (100), (011), (−111), (111), (002), (020), (–211), (–202), (220), (202), (013), (131), and (222), respectively, of the monoclinic phase of ZrO_2 (JCPDS File PDF No. 01-072-2743) [2,29]. The amount of m-ZrO_2 increased as the temperature was increased to 1,123 K, which shows that the sample was entirely in the monoclinic form. No other diffraction peaks were detected, indicating the purity of the prepared ZrO_2.

The average crystallite size of the prepared ZrO_2 was estimated by the Debye–Scherrer equation on the basis of the major peak of t-ZrO_2 (101) for 523 K and 823 K that of m-ZrO_2 was determined for 1,123 K. The crystallite sizes were found to be 5.1, 11.7, and 22.2 nm, respectively. This trend in particle size is in agreement with the crystal size theory hypothesized by Garvie, where the tetragonal form has a critical size smaller than that of the monoclinic phase [45]. The broad peak of the sample calcined at 523 K shown in the XRD

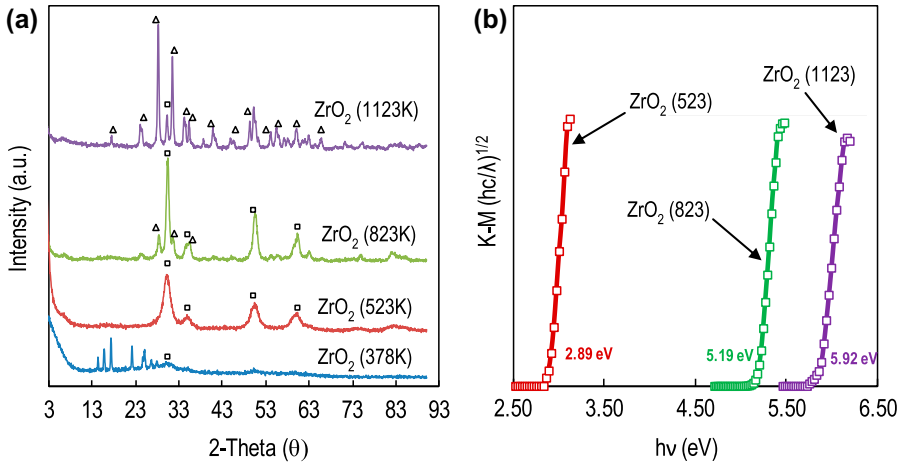

Fig. 1. XRD patterns for full range 3–93° (a) and the (f_{K-M}) vs. (hν) spectra (b) of ZrO_2 catalysts. The index symbol □: *t*-ZrO_2, △: *m*-ZrO_2.

results could also support this fact, indicating nano-sized *t*-ZrO_2 [46]. The lower free surface energy stabilized the *t*-ZrO_2 and disallowed its transformation to the monoclinic phase. However, increasing the temperature increased the crystallite size and zirconium destabilized, changing from the tetragonal to the monoclinic phase. Thus, it is expected that the *t*-ZrO_2 would give the best performance in the photocatalytic reaction of MB compared to *m*-ZrO_2 because smaller crystallite size always provides greater surface area [47].

3.1.2. Study of optical properties

The optical properties of the respective catalysts were studied by UV–vis diffuse reflectance spectroscopy (UV–vis/DRS). ZrO_2 exhibited a blue shift region, signifying the potential use of this catalyst in the photoreaction that conducted under UV irradiation. The band gap energy of ZrO_2 was determined using the Kubelka–Munk (K–M) spectrum by plotting $f_{K-M} = (hc/\lambda)^2$ as a function of $h\nu$; the results are shown in Fig. 1(b) [48]. The band gap value of the prepared ZrO_2 catalysts was similar and agreed with those reported in the literatures [49,50].

3.1.3. Morphological properties

The morphological properties of the ZrO_2 catalyst (523, 823, and 1,123 K) were examined by TEM; the images are presented in Fig. 2. It can be seen that the ZrO_2 particles were elliptical and irregular in shape, which may be due to particles overlapping [2,25]. The average particle size for these prepared ZrO_2 varied in a narrow range from 3 to 30 nm. The inset images show the fast Fourier transform patterns (FFT) and the magnification of the selected area in the FFT patterns show the atomic arrangement in the crystal to allow the estimation of the inter-planar distance. The inter-planar distance value (d_{101}) of the lattice fringes estimated (0.29 nm) from this image was consistent with the value of lattice spacing in ZrO_2, which was obtained from the XRD database software. In addition, the EDX analysis was employed to determine the composition of the ZrO_2 catalyst and result was tabulated in inset table in Fig. 2. The presence of Pt and C were corresponded to the coated material as well as the platform of the holder sample. No other element was detected indicating that the prepared ZrO_2 catalyst (523, 823, and 1,123 K) is free from other impurities.

3.1.4. Study of textural properties

The nitrogen adsorption–desorption isotherm of the *t*-ZrO_2 catalyst calcined at 523 K was examined and illustrated in Fig. 3(a). The isotherms showed a relative partial pressure (P/Po) hysteresis loop from 0.8 to 0.98. According to the IUPAC classification, this hysteresis loop follows the H1 type, which is the characteristic of solids consisting of particles composed of nearly cylindrical channels or made of aggregates or agglomerates of spherical particles [29]. Fig. 3(b) shows the cumulative pore volume distributions for the ZrO_2 catalyst, which resulted in a maximum pore volume diameter at ca. 60 Å. A total specific surface area of 83.7 $m^2 g^{-1}$ was obtained with the BET method.

3.1.5. Proposed mechanism of t-ZrO_2 formation

The reaction pathways for the formation of the ZrO_2 catalyst are proposed in Fig. 4. The electrolysis

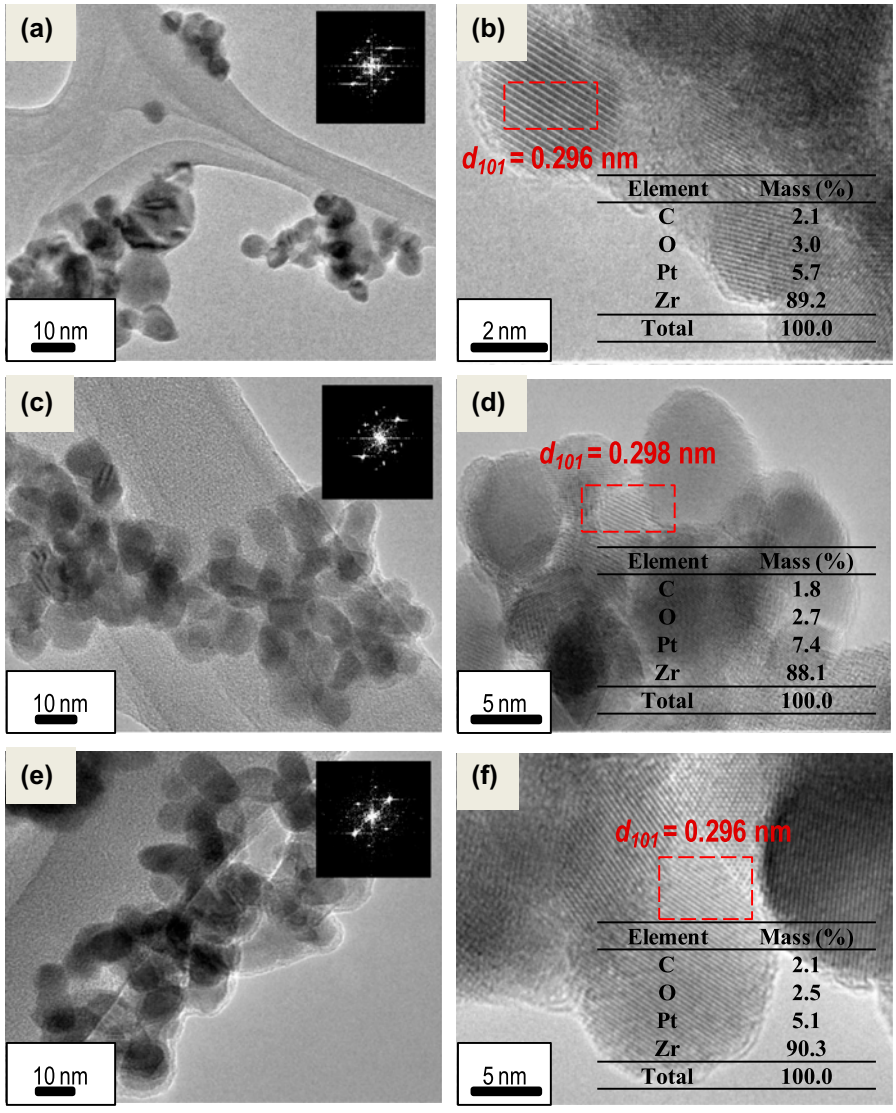

Fig. 2. TEM micrographs of ZrO_2 under calcination temperature of (a, b) 523 K, (c, d) 823 K, and (e, f) 1,123 K in low and high magnification, and the insert of Fig. 2(a, c, and e) are its corresponding FFT and the insert of Fig. 2(b, d, and f) are the EDX analysis of elemental composition of ZrO_2.

of a DMF solution with a Pt cathode and a Zr anode resulted in anodic dissolution of Zr metal to give Zr ions. On the other hand, electron transfer from naphthalene radical anions at the cathode, shown by the appearance of a dark green color on the surface of the cathode, also occurred to form pure nanometals (Zr^0), which were then oxidized to ZrO_2 during calcination [40].

The presence of a supporting electrolyte such as tetraalkylammonium salt might serve as a stabilizer for the metal clusters, which prevents metal agglomeration and the formation of undesired powders [51]. This resulted in a decrease in the particle size of ZrO_2, and finally led to the formation of the tetragonal phase when calcined at lower temperature [45].

3.2. Optimization and photocatalytic study

3.2.1. Quadratic model, regression, and surface response analysis

MB decolorization over the ZrO_2 catalyst was optimized using the RSM model with four factors, including pH (x_1), contact time (x_2), catalyst dosage (x_3), and calcination temperature (x_4). The list of experiments as designed by RSM and the value of the

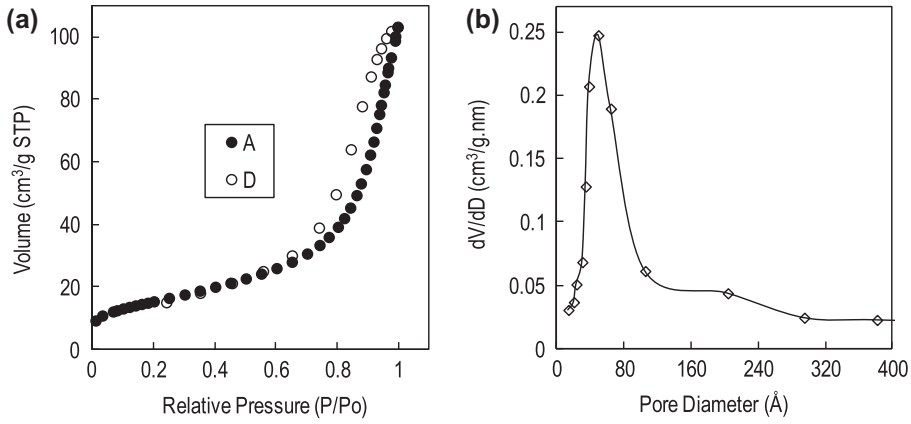

Fig. 3. The nitrogen adsorption–desorption isotherm (a), and Barrett–Joyner–Halenda (BJH) pore size distribution curve (b) of t-ZrO_2.

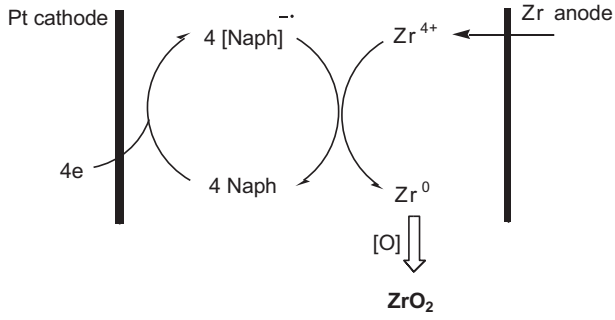

Fig. 4. Proposed mechanism for the formation of ZrO_2 catalyst.

response (decolorization percentage, %) for each sample obtained under the corresponding experimental conditions are shown in Table 3. The regression analysis was performed to fit the response, and the final regression function for the response in terms of coded factors utilized in the design of the statistical model is given as follows:

$$\begin{aligned} Y(\text{decolorization percentage, \%}) &= 2.1690 - 17.5078x_1 + 8.5424x_2 + 81.8255x_3 \\ &+ 0.0853x_4 + 1.6215x_1^2 - 1.2364x_2^2 - 34.2219x_3^2 \\ &+ 0.2171x_1x_2 + 2.3877x_1x_3 - 0.0055x_1x_4 \\ &- 0.2695x_2x_3 - 0.0010x_2x_4 - 0.0545x_3x_4 \end{aligned} \quad (4)$$

The ANOVA values of regression parameters for the predicted response surface quadratic model are tabulated in Table 4. The Fisher *F-test* demonstrated that the experimental results fitted well, and the model was significant, because of the model value F = 22.53 exceeded the table value $F_{(14,11,0.05)}$ = 2.72 with a low probability value ($P > F < 0$). The model terms are significant when the value of $P > F$ is less than 0.05, while values greater than 0.10 indicate that the model terms are not significant [42]. The quality of the model was evaluated on the basis of the value of R^2 which was relatively close to unity, in this case, equal to 0.97. This means that 97% of the variation in the decolorization of MB was explained by the independent variables, and the other 3% of the total variability in the response was not explained by the model. Therefore, the model was able to give a persuasively good estimate of the response in the considered range.

Residual analysis is one way to evaluate the validity of a model. A residual is defined as the difference between the observed value (actual) and the calculated value obtained from the model. A normal probability plot indicates that if the residuals follow a normal distribution then the points will follow a straight line. Fig. 5(a) shows a normal distribution of the studentized residuals, which are independent of each other. The straight line shows that the predicted values of MB obtained from the model and the actual experimental data were in good agreement. Fig. 5(b) represents the Pareto graphic analysis. This analysis reveals that all the factors were statistically significant with the calcination temperature (x_1), exhibiting a very strong influence on the examined response. The interactive effect of the pH (x_1), contact time (x_2), catalyst dosage (x_3), and calcination temperature (x_4) were represented by the three-dimensional response surface plot of percentage MB decolorization, as shown in Fig. 6.

The most important parameter that influenced the rate of the photocatalytic reaction was pH (x_1). During the reaction, it was difficult to interpret the effect of

Table 3
Experimental results for the four independent variables

Run No.	Factors (independent variables) x_1 pH	x_2 Contact time (h)	x_3 Catalyst dosage (g L^{-1})	x_4 Calcination temperature (K)	Response (% decolorization) Predicted	Actual
1	3	1	0.1	250	4.4	6.8
2	3	1	0.1	850	9.7	4.7
3	3	1	1.0	250	24.7	22.8
4	3	1	1.0	850	0.53	3.8
5	3	5	0.1	250	9.2	13.3
6	3	5	0.1	850	12.0	8.5
7	3	5	1.0	250	28.6	26.0
8	3	5	1.0	850	1.9	3.7
9	11	1	0.1	250	26.7	26.0
10	11	1	0.1	850	5.6	6.5
11	11	1	1.0	250	64.2	66.1
12	11	1	1.0	850	13.6	10.8
13	11	5	0.1	250	38.4	34.6
14	11	5	0.1	850	14.8	17.3
15	11	5	1.0	250	75.0	80.1
16	11	5	1.0	850	22.0	18.6
17	3	3	0.4	550	24.6	26.1
18	11	3	0.4	550	42.8	43.0
19	7	1	0.4	550	0.6	1.3
20	7	5	0.4	550	6.2	6.0
21	7	3	0.1	550	3.0	0.2
22	7	3	1.0	550	10.7	9.3
23	7	3	0.4	250	14.3	1.6
24	7	3	0.4	850	4.7	5.2
25 (C)	7	3	0.4	550	7.8	5.2
26 (C)	7	3	0.4	550	7.8	5.2

Table 4
ANOVA results for photodecolorization of MB and adequacy of the quadratic model

Source	Sum of squares	Degree of freedom	Mean square	*F*-value	*Prob* > *F*
x_1	2,008.97	1	2,008.97	89.87	0.000001
$(x_1)^2$	1,723.78	1	1,723.78	77.11	0.000003
x_2	193.38	1	193.38	8.65	0.013419
x_3	844.93	1	844.93	37.80	0.000072
x_4	2,564.24	1	2,564.24	114.71	0.000000
$(x_1)(x_3)$	299.20	1	299.20	13.38	0.003765
$(x_1)(x_4)$	693.32	1	693.32	31.02	0.000168
$(x_3)(x_4)$	877.14	1	877.14	39.24	0.000061
Regression	9,440.67	14	674.33	22.53	–
Residual	329.26	11	29.94		
Total	9,769.93	25	–		

F value (22.53) calculated > *F* value (2.72) from table, $R^2 = 0.9748$. $R^2_{adj} = 0.9428$.

pH because of its multiple roles including electrostatic interactions between the catalyst surface, solvent molecules, and substrate as well as charged radical formation [2]. Under alkaline conditions, poor competition mediated by the abundance of hydroxyl anions could render MB cations more easily attracted to the catalyst

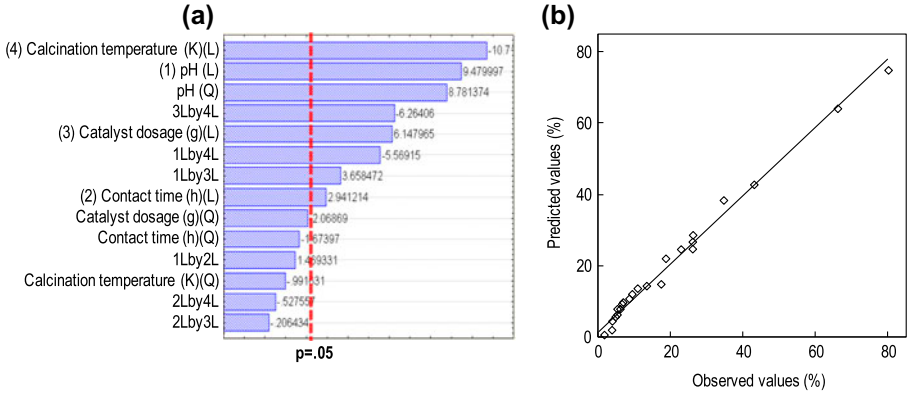

Fig. 5. Actual and predicted values of decolorization of MB ($R^2 = 0.97$) (a) and Pareto chart of standardized effect estimate (absolute value) (b).

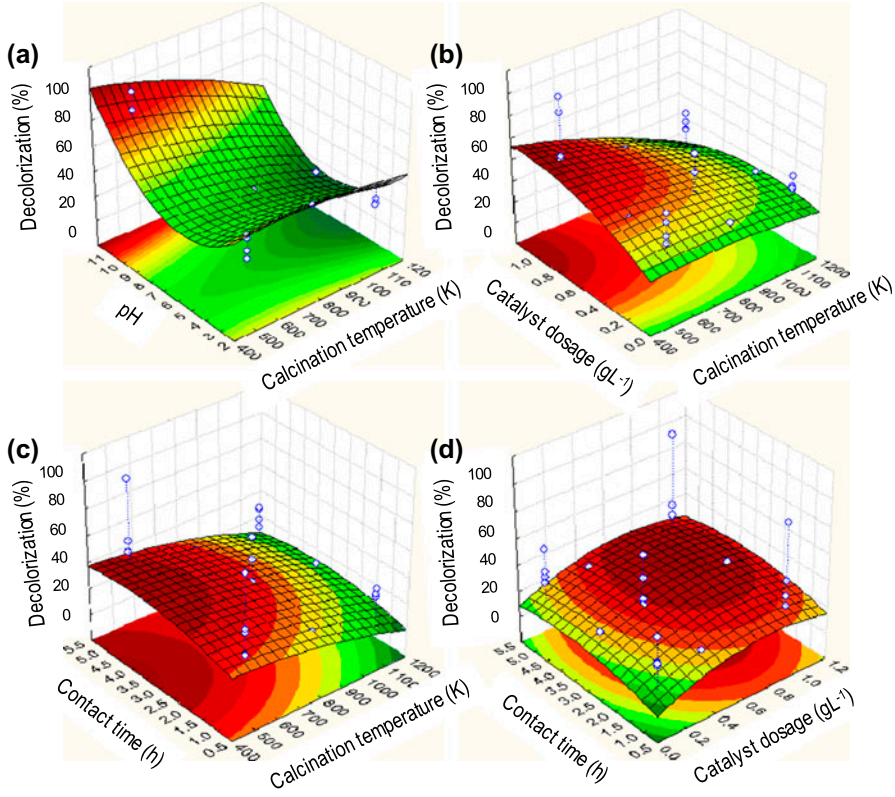

Fig. 6. Three-dimensional response surface plot of decolorization (%) of MB: interaction between (a) pH and calcination temperature, (b) catalyst dosage and calcination temperature, (c) contact time and calcination temperature, (d) contact time and catalyst dosage.

surface. The formation of hydroxyl radicals and the photocatalytic reaction rate was increased with exposure of this state to fluorescent light, leading to an increase in MB decolorization. Under acidic conditions, the competition between MB cations and H^+ ions occurred, which inhibited the dye from approaching the catalyst surface. Thus, the efficiency of the reaction reduced in comparison with alkaline conditions. Next, the number of active sites available on the catalyst also influenced the contact time (x_2) and catalyst dosage (x_3) [2,3]. The difference in calcination temperatures generated different types of

crystal growth of the ZrO_2 phase, as shown in Fig. 1(a). Significantly, the presence of the tetragonal phase (at 523 K) led to greater degradation of methylene blue compared to the monoclinic phase (Table 5).

3.2.2. Model validation and experimental confirmation

An actual experiment was conducted to validate the mathematical model generated during RSM implementation. The optimum conditions were used as generated by the DOE software, to confirm the validity of the predicted model and to optimize variables. In order to study the performance of each crystal phase of ZrO_2 transformation between the tetragonal and monoclinic phases, the effects of calcination temperature were taken into consideration. The experimental results are tabulated in Table 5, showing the high accuracy of the predicted values using Eq. (4). The transformation of ZrO_2 from the tetragonal to the monoclinic phase resulted in reduced MB degradation. An amount of 1.0 g L^{-1} ZrO_2 was found to be an optimum dosage for 10 mg L^{-1} MB, with 4 h of contact time at pH 11 which resulted in 84.9% decolorization as predicted by the theoretical value. The laboratory results indicated 83.6% MB decolorization, which is very close and fitted well with the optimized value generated by RSM.

3.3. Kinetic analysis

A series of reactions were performed using a calcination temperature of 523 K for the ZrO_2 catalyst to study the kinetics of MB photodecolorization, using the optimum conditions at pH 11 and different initial concentrations of MB ranging from 10 to 100 mg L^{-1} (Table 6). The result shows that the concentration of 10 mg L^{-1} gave the highest rate of decolorization (83.6%) after 4 h of irradiation. At a higher dye concentration, lower efficiency of photocatalytic decolorization was observed due to the formation of several layers of adsorbed dye on the catalyst surface and a reduction in direct contact of the catalyst with photogenerated holes or hydroxyl radicals [52]. This is also prevented the dye molecules from reaching the catalyst surface to adsorb light and photons.

The photocatalytic decolorization rate is commonly described by pseudo first-order kinetics, which is rationalized in terms of the Langmuir–Hinshelwood model, indicating reactions occurring at a solid–liquid interface [53,54]. The simplest equation for the rate of photodecolorization of MB is given by:

$$\ln C_t = -kt + \ln C_0 \tag{5}$$

where k is the pseudo first-order rate, and C_0 and C_t are the concentrations of MB at the start and

at time t, respectively. The integration of Eq. (5) yields Eq. (6):

$$\ln\left(\frac{C_0}{C_t}\right) = kt \tag{6}$$

The straight line of the plot of ln (C_0/C_t) as a function of time is shown in Fig. 7(a), and confirmed that reaction follows first-order kinetics; the slope of the line is the apparent first-order rate constant (k_{app}). The values of k obtained from these experiments are listed in Table 6. The higher first-order rate constant given by a lower concentration of MB indicates the suitability of the system for low dye concentrations. In reality, the concentration of dye in textile industry wastewater effluents is always in the range of 0.01–0.05 g L^{-1} [55].

The photodecolorization of MB by ZrO_2 could be an interface process [56], which might follow the Langmuir–Hinshelwood model (Eqs. (7) and (8)):

$$r_0 = -\frac{dC}{dt} = \frac{K_R K_{LH} C_0}{1 + K_{LH} C_0} = k_{app} C_0 \tag{7}$$

$$\frac{1}{k_{app}} = \frac{1}{K_R K_{LH}} + \frac{C_0}{K_R} \tag{8}$$

Table 5
Experimental results for model validation conducted at the optimum conditions as obtained from RSM

No.	pH	Contact time (h)	Catalyst dosage (g/L)	Calcination temperature (K)	Decolorization percentage	
					Predicted	Actual
1	11	4	1.0	523	84.9	83.6
2	11	4	1.0	823	74.8	72.9
3	11	4	1.0	1,123	64.7	61.5

Table 6
The parameters of photodecolorization at different initial concentration of MB

Initial concentration (mg L−1)	Reaction rate, k (min^{-1})	Initial reaction rate, r_o (mg L^{-1} min^{-1})	Decolorization (%)
10	0.0068	0.068	83.6
20	0.0048	0.096	60.0
30	0.0027	0.081	34.2
50	0.0017	0.085	22.1
70	0.0012	0.084	16.9
100	0.0009	0.090	14.1

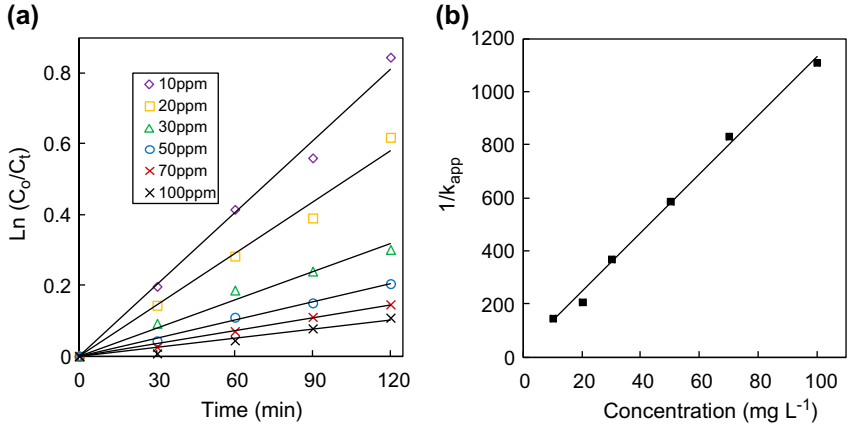

Fig. 7. Photodecolorization kinetics of MB using t-ZrO_2 at different MB concentrations (a) and the relationship between $1/k_{app}$ and initial concentration of MB (b).

where K_R is the reaction rate constant and K_{LH} is the Langmuir–Hinshelwood adsorption equilibrium constant.

Plotting $1/k_{app}$ as a function of C_0 (Fig. 7(b)) to give a linear plot verified that the photodecolorization of MB by ZrO_2 is consistent with the Langmuir–Hinshelwood model. The reaction rate constant and the adsorption equilibrium constant were calculated to be $K_R = 0.09$ mg L^{-1} min^{-1} and $K_{LH} = 0.43$ L mg^{-1}, respectively. These results suggest that the reaction occurs in the bulk of the solution as well as at the surface of the catalyst because the value of K_{LH} was greater than K_R [57]. The presence of some chloride ions in the water most probably blocked the adsorbing sites of the catalyst and thus, competitively inhibit adsorption of hydroxide to produce hydroxyl radicals [57] However, in our experiment deionized water was used throughout and the concentrations of residual anions should be very low. If anions of such a concentration level as in deionized water can lead to severe anion inhibition, photocatalytic oxidation might be commercially impractical.

3.4. Regeneration and comparison of performance study

Fig. 8 shows the regeneration study using the t-ZrO_2 (523 K) catalyst in terms of the photocatalytic activity of MB decolorization. The experimental conditions described above were used. The initial concentration of MB was held constant at 10 mg L^{-1} at pH 11 and 4 h of irradiation time. Then, the catalyst was regenerated after filtration and calcination at 523 K for 3 h after every cycle. A slight decrease <10% was observed with no obvious catalyst deactivation, indicating that the reaction could be maintained after five cycling runs [2,3,38].

The proficiency of photoactivity and a comparison study was conducted using prepared t-ZrO_2, commercial t-ZrO_2, Degussa P22 TiO_2 as well as photolysis reaction (Fig. 9). The result shows that under photolysis condition only 10% MB was decolorized, this may be due to the long exposure to the UV-light. While, the prepared t-ZrO_2 showed the greatest photoactivity toward MB decolorization (up to 83.6%), followed by Degussa P25 TiO_2 (64.5%), and the commercial t-ZrO_2

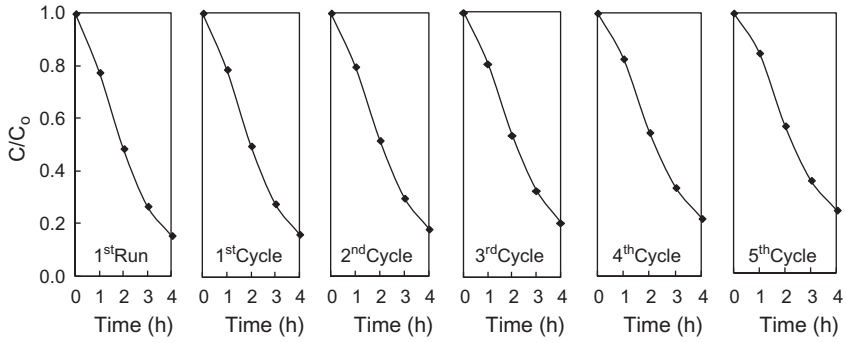

Fig. 8. Regeneration of *t*-ZrO_2 on photocatalytic decolorization of MB. [$C_0 = 10$ mg L^{-1}, pH = 11, $W = 1.0$ g L^{-1}, $t = 4$ h, 303 K].

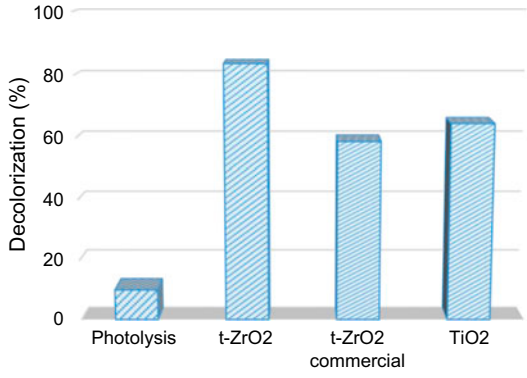

Fig. 9. Comparison in the performance of catalysts in the photocatalytic decolorization of MB. [$C_0 = 10$ mg L^{-1}, pH = 11, $W = 1.0$ g L^{-1}, $t = 4$ h, 303 K].

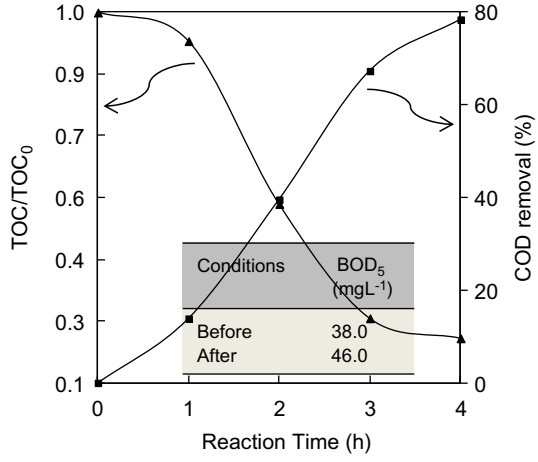

Fig. 10. The graph of COD removal and TOC reduction levels after 4 h of reaction, and the insert table are its corresponding BOD_5. [$C_0 = 10$ mg L^{-1}, pH = 11, $W = 1.0$ g L^{-1}, $t = 4$ h, 303 K, Catalyst used = *t*-ZrO_2].

(58.7%) catalyst. This efficiency may be due to the surface area of each catalyst, in which the prepared *t*-ZrO_2, commercial, and *t*-ZrO_2 Degussa P22 TiO_2 possess 83.7, 18.4, and 10.5 m^2 g^{-1}, respectively.

3.5. Investigation on biodegradability

The measurement of chemical oxygen demand (COD), total organic carbon (TOC), and five day biochemical oxygen demand (BOD_5) for the MB solution was carried out; the results are shown in Fig. 10. To investigate the amount of organic compounds that were present in the aqueous solution, the COD test was performed. The result was initially measured as 144 mg L^{-1}, and after 4 h irradiation, and was reduced gradually to 31 mg L^{-1}. On the other hand, the significant decrease in the total organic carbon ratio (TOC/TOC_0) demonstrated that mineralization occurred during the irradiation process, indicating that the dye molecules were fragmented and converted into small organic molecules [2]. The biodegradability index for the aqueous dye solution can be measured using the BOD_5/COD ratio, which for the non-irradiated dye solution was 0.26, indicating that the dye solution is non-biodegradable [58]. The BOD_5/ COD ratio increased up to 1.48 after 4 h of irradiation, demonstrating the formation of more biodegradable intermediates following photodegradation [59]. In addition, changes in pH were also monitored before and after the reaction, and changed from pH 11 to pH 8, respectively. This change illustrated the possible mineralization of MB dye to some extent into CO_2 and H_2O [60].

4. Conclusion

In conclusion, we have demonstrated that the *t*-ZrO_2 catalyst synthesized by electrochemical method could be stabilized at low calcination temperature without the addition of a dopant in the preparation

step. XRD result revealed the mere existence of t-ZrO_2 at 523 K, suggesting the TEAP most probably plays important role for the stabilization by preventing the agglomeration of metal clusters with undesired powders in the electrolysis system, resulting in a decrease in ZrO_2 crystal size. Increasing the calcination temperature increased the crystallite size which then changed the phase of ZrO_2 from tetragonal to monoclinic phase. The prepared t-ZrO_2 showed the highest photoactivity (83.6%) on the decolorization of MB as compared with Degussa P25 TiO_2 (64.5%) and the commercial t-ZrO_2 (58.7%). Optimization on the photodecolorization of MB by RSM gave 1.53% errors to experimental value, indicating that the model provided a good estimation of the response in the considered range. The good stability after five cycling runs as well as good mineralization of MB, demonstrating the potential use of t-ZrO_2 in dye wastewater treatment.

Acknowledgments

The authors are grateful for the financial support by Research University Grant from the Universiti Teknologi Malaysia (grant number 4L112), the awards of the UTM Zamalah Scholarship (Norzahir Sapawe) and the Hitachi Scholarship Foundation for their support.

References

[1] N.M. Mahmoodi, Manganese ferrite nanoparticle: Synthesis, characterization, and photocatalytic dye degradation ability, Desalin. Water Treat. (2013), doi:10.1080/19443994.834519.

[2] N. Sapawe, A.A. Jalil, S. Triwahyono, S.H. Adam, N.F. Jaafar, M.A.H. Satar, Isomorphous substitution of Zr in the framework of aluminosilicate HY by an electrochemical method: Evaluation by methylene blue decolorization, Appl. Catal. B: Environ. 125 (2012) 311–323.

[3] N.F. Jaafar, A.A. Jalil, S. Triwahyono, M.N.M. Muhid, N. Sapawe, M.A.H. Satar, H. Asaari, Photodecolorization of methyl orange over α–Fe_2O_3–supported HY catalysts: The effects of catalyst preparation and dealumination, Chem. Eng. J. 191 (2012) 112–122.

[4] A.A. Jalil, S. Triwahyono, S.H. Adam, N.D. Rahim, M.A.A. Aziz, N.H.H. Hairom, N.A.M. Razali, M.A.Z. Abidin, M.K.A. Mohamadiah, Adsorption of methyl orange from aqueous solution onto calcined Lapindo volcanic mud, J. Hazard. Mater. 181 (2010) 755–762.

[5] A.A. Jalil, S. Triwahyono, N.A.M. Razali, N.H.H. Hairom, A. Idris, M.N.M. Muhid, A. Ismail, N.A.M. Yahaya, N.A.L. Ahmad, H. Dzinun, Complete electrochemical dechlorination of chlorobenzenes in the presence of various arene mediators, J. Hazard. Mater. 174 (2010) 581–585.

[6] C.S.D. Rodrigues, L.M. Madeira, R.A.R. Boaventura, Treatment of textile effluent by chemical (Fenton's Reagent) and biological (sequencing batch reactor) oxidation, J. Hazard. Mater. 172 (2009) 1551–1559.

[7] F. Harrelkas, A. Azizi, A. Yaacoubi, A. Benhammou, M.N. Pons, Treatment of textile dye effluents using coagulation–flocculation coupled with membrane processes or adsorption on powdered activated carbon, Desalination 235 (2009) 330–339.

[8] R.A. Damodar, S.J. You, S.H. Ou, Coupling of membrane separation with photocatalytic slurry reactor for advanced dye wastewater treatment, Sep. Pur. Technol. 78 (2010) 64–71.

[9] J.S. Wu, L.H. Liu, K.H. Chu, S.Y. Suen, Removal of cationic dye methyl violet 2B from water by cation exchange membranes, J. Membr. Sci. 309 (2008) 239–245.

[10] S. Liu, Y. Cai, X. Cai, H. Li, F. Zhang, Q. Mu, Y. Liu, Y. Wang, Catalytic photodegradation of Congo red in aqueous solution by $Ln(OH)_3$ (Ln=Nd, Sm, Eu, Gd, Tb, and Dy) nanorods, Appl. Catal. A: Gen. 453 (2013) 45–53.

[11] N. Sapawe, A.A. Jalil, S. Triwahyono, M.I.A. Shah, R. Jusoh, N.F.M. Salleh, B.H. Hameed, A.H. Karim, Cost-effective microwave rapid synthesis of zeolite NaA for removal of methylene blue, Chem. Eng. J. (2013) 388–398.

[12] S.M. Lum, J.C. Sin, A.Z. Abdullah, A.R. Mohamed, Degradation of wastewaters containing organic dyes photocatalysed by zinc oxide: A review, Desalin. Water. Treat. 41 (2012) 131–169.

[13] D. Robert, Photosensitization of TiO_2 by M_xO_y and M_xS_y nanoparticles for heterogeneous photocatalysis applications, Catal. Today 122 (2007) 20–26.

[14] N. Talebian, M.R. Nilforoushan, Comparative study of the structural, optical and photocatalytic properties of semiconductor metal oxides toward degradation of methylene blue, Thin Solid Films 518 (2010) 2210–2215.

[15] M. Aleksic, H. Kusic, N. Koprivanac, D. Leszczynska, A.L. Bozic, Heterogeneous fenton type processes for the degradation of organic dye pollutant in water: The application of zeolite assissted AOPs, Desalination 257 (2010) 22–29.

[16] M. Gurulakshmi, M. Selvaraj, A. Selvamani, P. Vijayan, N.R. Sasi-Rekha, K. Shanthi, Enhanced visible-light photocatalytic activity of V_2O_5/S-TiO_2 nanocomposites, Appl. Catal. A: Gen. 449 (2012) 31–46.

[17] S. Yamazaki, T. Yamate, K. Adachi, Photocatalytic activity of aqueous WO_3 sol for the degradation of Orange II and 4-chlorophenol, Appl. Catal. A: Gen. 454 (2013) 30–36.

[18] M. Pelaez, N.T. Nolan, S.C. Pillai, M.K. Seery, P. Falaras, A.G. Kontos, P.S.M. Dunlop, J.W.J. Hamilton, J.A. Byrne, K. O'Shea, M.H. Entezari, D.D. Dionysiou, A review on the visible light active titanium dioxide photocatalysts for environmental applications, Appl. Catal. B: Environ. 125 (2012) 331–349.

[19] A. Nezamzadeh-Ejhieh, M.K. Shamsabadi, Decolorization of a binary azo dyes mixture using CuO incorporated nanozeolite-X as a heterogeneous catalyst and solar irradiation, Chem. Eng. J. 228 (2013) 631–641.

[20] A. Nezamzadeh-Ejhieh, H. Zabihi-Mobarakeh, Heterogeneous photodegradation of 2,4-dichlorophenol using FeO doped onto nano-particles of zeolite P, J. Ind.

Eng. Chem. (2013), Available from http://dx.doi.org/10.1016/j.jiec.2013.03.035.
[21] J.A. Khan, X. He, H.M. Khan, N.S. Shah, D.D. Dionysiou, Oxidative degradation of atrazine in aqueous solution by UV/H_2O_2/Fe^{2+}, UV/$S_2O_8^{2-}$/Fe^{2+} and UV/HSO_5^-/Fe^{2+} processes: A comparative study, Chem. Eng. J. 218 (2013) 376–383.
[22] A. Nezamzadeh-Ejhieh, S. Hushmandrad, Solar photodecolorization of methylene blue by CuO/X zeolite as a heterogeneous catalyst, Appl. Catal. A: Gen. 388 (2010) 149–159.
[23] A. Nezamzadeh-Ejhieh, Z. Salimi, Heterogeneous photodegradation catalysis of *o*–phenylenediamine using CuO/X zeolite, Appl. Catal. A: Gen. 390 (2010) 110–118.
[24] A. Nezamzadeh-Ejhieh, Z. Banan, A comparison between the efficiency of CdS nanoparticles/zeolite A and CdO/zeolite A as catalysts in photodecolorization of crystal violet, Desalination 279 (2011) 146–151.
[25] N. Chandra, D.K. Singh, M. Sharma, R.K. Upadhyay, S.S. Amritphale, S.K. Sanghi, Synthesis and characterization of nanosized zirconia powder synthesized by single emulsion–assisted direct precipitation, J. Colloid Interface Sci. 342 (2010) 327–332.
[26] J.A. Moreno, G. Poncelet, Isomerization of *n*-butane sulfated Al- and Ga-promoted zirconium oxide catalysts. Influence of promoter and preparation method, J. Catal. 203 (2001) 453–465.
[27] C. Morterra, G. Cerrato, F. Pinna, M. Signoretto, Crystal phase, spectral features, and catalytic activity of sulfate-doped zirconia systems, J. Catal. 157 (1995) 109–123.
[28] R. Srinivasan, C.R. Hubbard, O.B. Cavin, B.H. Davis, Factors determining the crystal phases of zirconia powders: A new outlook. Chem. Mater. 5 (1993) 27–31.
[29] Q. Chang, J.-E. Zhou, Y. Wang, G. Meng, Preparation and characterization of unique zirconia crystal within pores via sol–gel–hydrothermal method, Adv. Powder Technol. 20 (2009) 371–374.
[30] C.A. Kawaguti, L.A. Chiavacci, S.H. Pulcinelli, C.V. Santilli, V. Briois, Structural features of phosphate and sulfate modified zirconia prepared by sol–gel route, J. Sol–Gel Sci. Technol. 32 (2004) 91–97.
[31] A. Gulino, S. La Delfa, I. Fragala, Low-temperature stabilization of tetragonal zirconia by bismuth. Chem. Mater. (1996) 1287–1291.
[32] M. Rezaei, S.M. Alavi, S. Sahebdelfar, Z.–F. Yan, Tetragonal nanocrystalline zirconia powder with high surface area and mesoporous structure, Powder Technol, 168 (2006) 59–63.
[33] F. Heshmatpour, R.B. Aghakhanpour, Synthesis and characterization of superfine pure tetragonal nanocrystalline sulfated zirconia powder by a non-alkoxide sol–gel route, Adv. Powder Technol. 23 (2012) 80–87.
[34] R. Dwivedi, A. Maurya, A. Verma, R. Prasad, K.S. Bartwal, Microwave assited sol–gel synthesis of tetragonal zirconia nanoparticles, J. Alloys Compd. 509 (2011) 6848–6851.
[35] H.–J. Huang, M.–C. Wang, The phase formation and stability of tetragonal ZrO_2 prepared in a silica bath, Ceram. Int, 39 (2013) 1729–1739.
[36] R.A. Rocha, E.N.S. Muccillo, L. Dessemond, E. Djurado, Thermal ageing of nanostructured tetragonal zirconia ceramics: Characterization of interfaces, J. Eur. Ceram. Soc. 30 (2010) 227–231.
[37] A.A. Jalil, M.A.H. Satar, S. Triwahyono, H.D. Setiabudi, N.H.N. Kamarudin, N.F. Jaafar, N. Sapawe, R. Ahamad, Tailoring the current density to enhance photocatalytic activity of CuO/HY for decolorization of malachite green, J. Electroanal. Chem. (2013) 50–58.
[38] N. Sapawe, A.A. Jalil, S. Triwahyono, R.N.R.A. Sah, N.W.C. Jusoh, N.H.H. Hairom, J. Efendi, Electrochemical strategy for grown ZnO nanoparticles deposited onto HY zeolite with enhanced photodecolorization of methylene blue: Effect of the formation of Si–O–Zn bonds, Appl. Catal. A: Gen. 456 (2013) 144–158.
[39] A.A. Jalil, N. Kurono, M. Tokuda, Facile synthesis of 2-arylpropenoic acid esters by cross-coupling using electrogenerated highly reactive zinc and a palladium catalyst, Synlett. 12 (2001) 1944–1946.
[40] A.A. Jalil, N. Kurono, M. Tokuda, Facile synthesis of ethyl–2–arylpropenoates by cross-coupling reaction using EG-highly reactive zinc, Tetrahedron 58 (2002) 7477–7484.
[41] A.A. Jalil, N. Kurono, M. Tokuda, Synthesis of the precursor of anti-inflammatory agents by cross-coupling using electrogenerated highly reactive zinc, Synthesis 18 (2002) 2681–2686.
[42] Y.L. Pang, A.Z. Abdullah, S. Bhatia, Optimization of sonocatalytic degradation of Rhodamine B in aqueous solution in the presence of TiO_2 nanotubes using response surface methodology, Chem. Eng. J. 166 (2011) 873–880.
[43] W. Jiang, J.A. Joens, D.D. Dionysiou, K.E. O'Shea, Optimization of photocatalytic performance of TiO_2 coated glass microspheres using response surface methodology and the application for degradation of dimethyl phthalate, J. Photochem. Photobiol. A: Chem. 262 (2013) 7–13.
[44] J. Dostanic, D. Loncarevic, L. Rozic, S. Petrovic, D. Mijin, D.M. Jovanovic, Photocatalytic degradation of azo pyridone dye: Optimization using response surface methodology, Desalin. Water Treat. 51 (2013) 2802–2812.
[45] R.C. Garvie, The occurrence on metastable tetragonal zirconia as a crystallite size effect, J. Phys. Chem. 69 (1965) 1238–1243.
[46] N.C.S. Selvam, A. Manikandan, L.J. Kennedy, J.J. Vijaya, Comparative investigation of zirconium oxide (ZrO_2) nano and microstructures for structural, optical and photocatalytic properties, J. Colloid Interface Sci. 389 (2013) 91–98.
[47] J.N. Park, J. Noh, J.S. Chang, S.E. Park, Ethylbenzene to styrene in the presence of carbon dioxide over zirconia, Catal. Lett. 65 (2000) 75–78.
[48] H. Jia, H. Xu, Y. Hu, Y. Tang, L. Zhang, TiO_2@CdS core–shell nanorods films: Fabrication and dramatically enhanced photoelectrochemical properties, Electrochem. Commun. 9 (2007) 354–360.
[49] J. Portier, H.S. Hilal, I. Saadeddin, S.J. Hwang, M.A. Subramanian, G. Campet, Thermodynamic correlations and band gap calculations in metal oxides, Prog. Solid State Chem. 32 (2004) 207–217.
[50] C.R. Foschini, O.T. Filho, S.A. Juiz, A.G. Souza, J.B.L. Oliveira, E. Longo, E.R. Leite, C.A. Paskocimas, J.A. Varela, On the stabilizing behavior of zirconia: A Combined experimental and theoretical study, J. Mater. Sci. 39 (2004) 1935–1941.

[51] M.T. Reetz, W. Helbig, Size-selective synthesis of nanostructured transition metal clusters, J. Am. Chem. Soc. 116 (1994) 7401–7402.
[52] H. Lachheb, E. Puzenat, A. Houas, M. Ksibi, E. Elaloui, C. Guillard, J.M. Herrmann, Photocataytic degradation of various types of dyes (Alizarin S, Crocein Orange G, Methyl Red, Congi Red, Methylene Blue) in water by UV–irradiated titinia, Appl. Catal. B: Environ. 39 (2002) 75–90.
[53] M. Montazerozohori, S.M. Jahromi, Photocatalytic decolorization of ethyl orange at various buffer solutions using nano-titanium dioxide: A kinetic investigation, Desalin. Water Treat. 48 (2012) 261–266.
[54] Z. Mesgari, M. Gharagozlou, A. Khosravi, K. Gharanjig, Synthesis, characterization and evaluation of efficiency of new hybrid Pc/Fe-TiO_2 nanocomposite as photocatalyst for decolorization of methyl orang using visible light irradiation, Appl. Catal. A: Gen. 411–412 (2012) 139–145.
[55] J. Grzechulska, A.W. Morawski, Photocatalytic decomposition of azo–dye acid black 1 in water over modified titanium dioxide. Appl. Catal. B: Environ. 36 (2002) 45–51.
[56] L.Y. Yang, S.Y. Dong, J.H. Sun, J.L. Feng, Q.H. Wu, S.P. Sun, Microwave-assisted preparation, characterization and photocatalytic properties of a dumbbell-shaped ZnO photocatalyst, J. Hazard. Mater. 179 (2010) 438–443.
[57] J. Cunningham, G. Al–Sayyed, Factors influencing efficiencies of TiO_2-sensitised photodegradation. Part 1-Substituted benzoic acids: Discrepancies with dark-adsorption parameters, J. Chem. Soc. Faraday Trans. 86 (1990) 3935–3941.
[58] Y. Meng, X. Huang, Y. Wu, X. Wang, Y. Qian, Kinetic study and modeling on photocatalytic degradation of para-chlorobenzoate at different light intensities, Environ. Pollut. 117 (2002) 307–313.
[59] K. Swaminathan, K. Pachhade, S. Sandhya, Decomposition of a dye intermediate, (H-acid) 1 amino-8-naphthol-3,6 disulfonic acid in aqueous solution by ozonation, Desalination 186 (2005) 155–164.
[60] N. Sapawe, A.A. Jalil, S. Triwahyono, One-pot electrosynthesis of ZrO_2-ZnO/HY nanocomposite for photocatalytic decolorization of various dye-contaminants, Chem. Eng. J. 225 (2013) 254–265.